Sixth International Conference on Durability of Concrete Structures **Paper Number KN06**
18 - 20 July 2018
University of Leeds, Leeds, West Yorkshire, LS2 9JT, United Kingdom

Analytical and Quantitative Aspects of Surface Moisture Transport and Plastic Shrinkage Cracking

B. Mobasher
School of Sustainable Engineering and the Built Environment, Arizona State University, Tempe, USA

M. Bakhshi
AECOM, New York, USA

Y. Yao
College of Civil Engineering, Southeast University, Nan Jing, China

ABSTRACT

The drying rate of porous materials such as hydrating cement paste during early hydration stages is studied using analytical and experimental procedures. Effects of micro and macro fibers as they change the nature of restrained shrinkage cracking are also documented. A methodology based on vacuum drying experiments is developed to measure the rate of evaporation from the surface of fresh paste and mortar mixtures that leads to restrained shrinkage cracking. Stages of microcrack coalescence due to plastic shrinkage cracking are quantitatively analyzed using digital image correlation. A model for internal moisture transfer simulates initial constant drying rate followed by a vapor diffusion transport phenomena.

A fluid mechanics approach for water evaporation from the boundary-layer in terms of mass transfer, diffusion, and convection is used. Effect of temperature, wind speed, and relative humidity are studied. Results of these two experiments are then integrated with an analytical approach for the restrained ring specimen which correlates the moisture diffusion in the specimen with the rate of evaporation and shrinkage strain. The model incorporates key influential parameters of diffusion, evaporation, shrinkage, creep, aging, and microcracking, in the stress analysis of a restrained concrete section. The formulation addresses the effect of geometry of the specimen, the humidity and shrinkage conditions, and the restraint offered by stiffness of the steel ring. Finally the modelling is extended to simulate a slab on ground and predict multiple transverse cracking as well as slab curling using a finite difference model.

Keywords: restrained shrinkage, cracking, drying, diffusion, moisture transport, modeling

1.0 INTRODUCTION

Surface of freshly-placed concrete when restrained and exposed to drying conditions is susceptible to early age plastic shrinkage cracks. Guidelines for durable concrete therefore require addressing of crack widths. Passageways such as cracks and joints lead to eventual transport of ions and removal of barriers that prevent infiltration of harmful ions. Early age properties such as shrinkage and thermal dimensional changes are key parameters in reducing the potential long-term durability in structural design.

Even at relatively low volumes, fibers are effective in controlling the cracking of plastic concrete (ACI Committee 224, 2007; ACI Committee 302, 2004) by increasing the strength and strain capacity during early ages and minimize the potential for cracking due to the tensile stresses generated by the shrinkage (ACI Committee 544, 2010). Fibers inhibit crack propagation by providing bridging forces across the crack surfaces (Grzybowski and Shah, 1990; Kim *et al.*, 2008). They also indirectly influence plastic shrinkage cracking and the evaporation rate by increasing crack density and reducing their width.

Initiated by high rate of water evaporation from the exposed surface (Banthia and Gupta, 2009; Cohen *et al*., 1990; Mora-Ruacho *et al.*, 2009) plastic shrinkage cracks reduce load carrying capacity, allow ingress of aggressive agents, increase maintenance costs, and reduce service life (Kwon *et al.*, 2009; Mu and Forth, 2009; Yoon *et al.*, 2007). From a diagnostic point of view, we have primarily used the well-known Menzel formula, developed based on water evaporation rate from the surface a lake Hefner, for more than 60 years ago. There is a need to employ scientific approaches that rely on key mechanisms and allow for mix design parameters to be included in the solution strategy.

Effective prevention techniques rely on prevention of water loss, thus the mechanisms of evaporation from

the surface given the moisture transport phenomenon is essential in effective control of plastic shrinkage cracks (Banthia *et al.*, 1993; Banthia and Yan, 2000; Grzybowski and Shah, 1990; Qi *et al.,* 2003). During the drying phase, moisture flows through the porous material towards the evaporative surface to supply the necessary surface flux. Diffusion of water through the boundary layer to the surface maintains the equilibrium of liquid-gas phase transition (Arya, 2001; Brighton, 1985; Brutsaert, 1965; Huang, 1997; Prata and Sparrow, 1985; Sultan *et al.*, 2005). The interaction of unsaturated flow within pores and surface evaporation rate can be used to measure moisture diffusivity (Carmeliet *et al.*, 2004; Janz, 1997).

Key factors of plastic shrinkage potential include wind velocity and temperature as they correlate with surface conditions of concrete and its rate of drying. This rate can be obtained from the moisture movement due to the porosity and capillary porosity of the freshly poured mix and allows for determination of degree of potential for bleeding/cracking. The interaction of bleeding and evaporation are modelled by means of nonlinear fluid mechanics, gas transport to the surface and the subsequent evaporation.

2.0 LOW PRESSURE DRYING EXPERIMENTS

Effect of fibers on the moisture loss and evaporation rate were studied by Bakhshi and Mobasher using low-pressure drying tests as shown in Fig. 1 to study the shrinkage cracking of fresh cement paste (Dey *et al.*, 2015). This test method uses a low-pressure vacuum to monitor weight-loss and mass transfer properties during the early drying stages while the development of crack patterns during drying is documented using time-lapse photography. Reduction of crack areal fraction due to increase in the fiber content can be quantitatively measured. Rate of evaporation, weight loss, surface cracking, and mass transfer coefficients are obtained using analytical methods by relating moisture diffusivity to the effect of fibers on apparent diffusion coefficients. As shown in Figs. 2(a) and 2(b), moisture evaporation rate is simulated using a dual-stage drying model and moisture diffusivity constants representing liquid and vapor phases (Dey *et al.*, 2016).

Figure 2 relates the temporal cumulative moisture loss and evaporation flux (Dey *et al.*, 2016). Drying in Stage I is a continuous liquid phase within the pore structure, while Stage II describes a discontinuous liquid-continuous vapor phase within the pore structure. Moisture removal in Stage II is dominated by diffusion coefficient of the internal microstructure, such that the evaporation rate reduces and moisture content decreases below saturation. Shrinkage cracks occur when the biaxial tension shrinkage stresses exceed the uniaxial tensile strength.

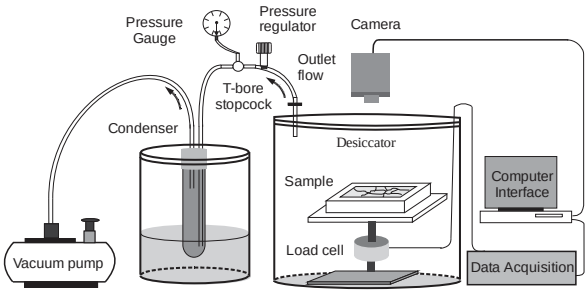

Fig. 1. Schematic of vacuum drying test setup

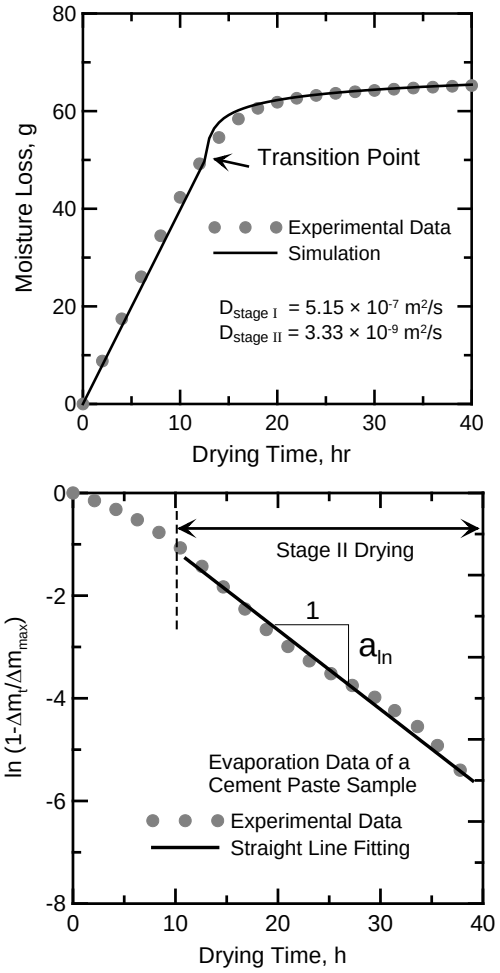

Fig. 2. (a) Experimental moisture loss and its Simulation for cement paste (b) Derivation of model coefficients for linearized curve of moisture loss $\ln\left(1-\Delta M_t / \Delta M_{\max}\right)$ vs. time in stage II.

Figure 3 shows the surface deformation and associated strain distribution. In addition, maximum crack width was significantly reduced (approximately 50-70%) in comparison to control samples. Map cracking on the surface and its morphology are shown.

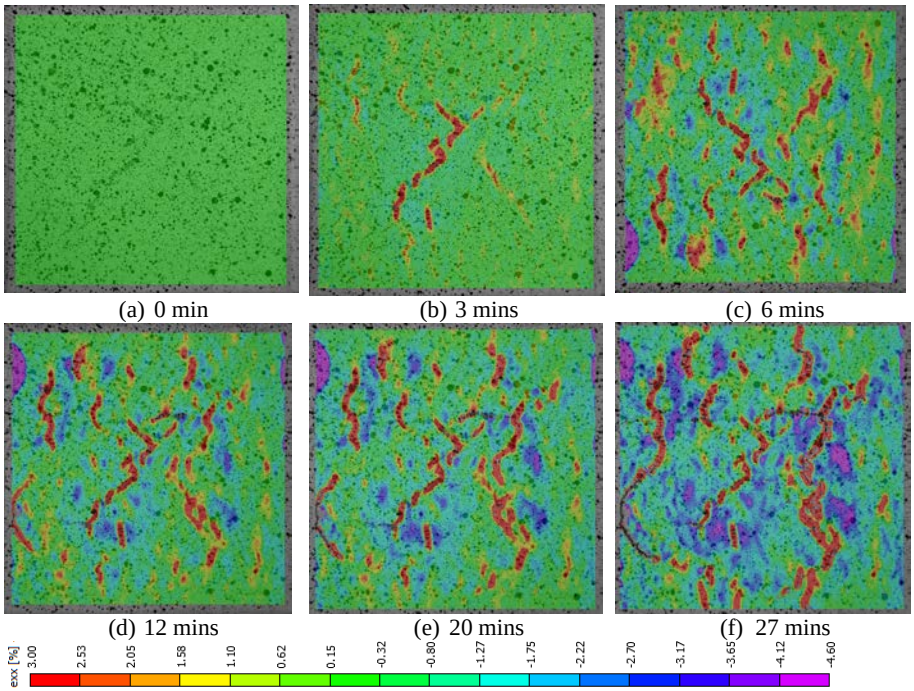

Fig. 3: Sequential growth of shrinkage cracks observed in an alkali activated slag specimen within the first hour of the test (Dey *et al.*, 2015).

Comparison of micro and macro wollastonite micro-fibers with the control matrix as shown in Fig. 4. The time history of total cracked area during the experiment shows crack initiation within 2 hours and crack saturation within 5 hours. Progression of cracks is much faster in the control specimen and addition of coarse (C850 and C2000, representing mean fiber length in microns) and fine grained (F33, F55) wollastonite microfibers both the rate and extent of the crack area are reduced. Use of fine grained fibers result in the lowest crack formation rate (defined as crack area change per unit time), an order of magnitude lower rate than control paste. Relationship between crack area and cumulative moisture loss is expressed as a linear function as shown in Fig. 4b.

3.0 FLUID MECHANICS-BASED ESTIMATION OF EVAPORATION RATE

Using a fluid mechanics approach, the evaporation rate is modelled with four main input parameters of temperature, RH, wind velocity, and moisture diffusion rate. The analytical model is based on two coupled mechanisms and integrates boundary layer theory with diffusion and convection mass transfer (Bakhshi *et al.*, 2012). The first set of equations address the mass transfer and diffusion of water vapor from the pore to the surface in order to maintain a finite thickness boundary layer.

The second component is the convection, primarily due to temperature and wind at the boundary layer. The model validation is by predicting the evaporation rate during the stage I, from a smooth isothermal flat plate with an external forced convection mass transfer is then coupled with the internal diffusion as shown in Figs. 5(a) and 5(b).

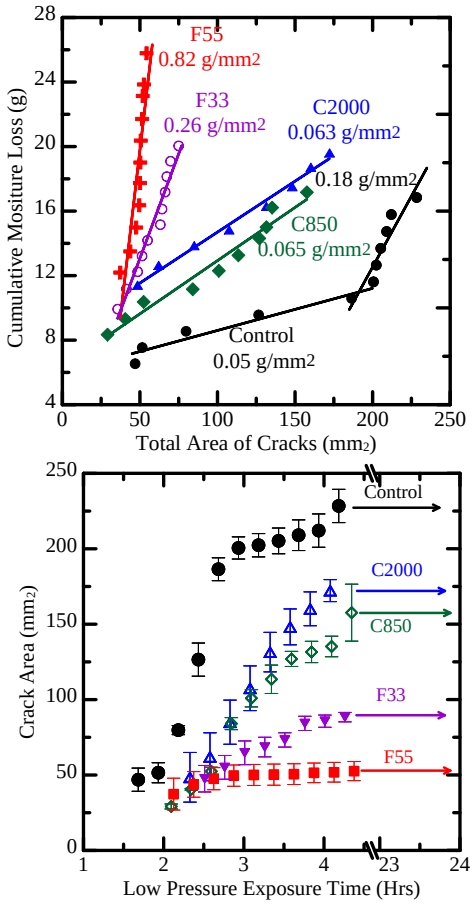

Fig. 4. a) Effect of wollastonite micro-reinforcement in crack formation, b) Correlation of moisture loss and crack morphology

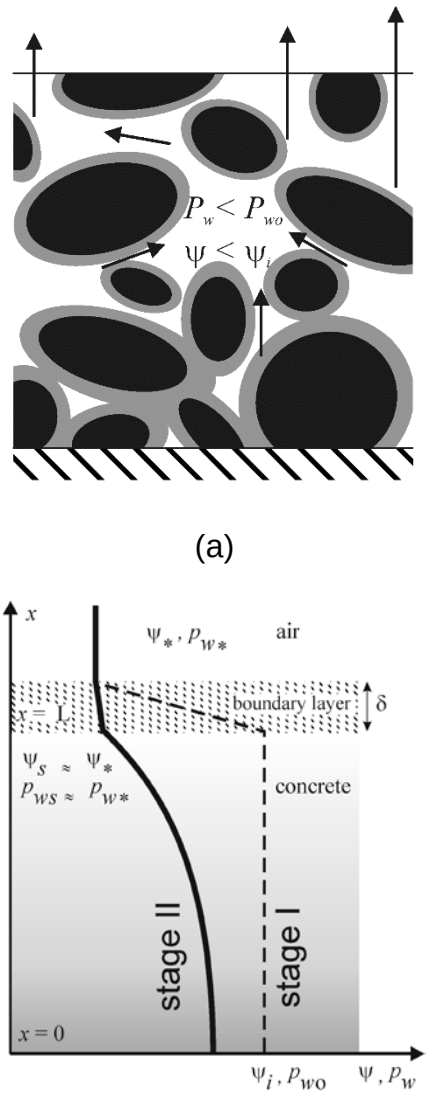

Fig. 5. (a) Low saturation state of porous material as the advanced stage of drying, (b) variation of hydraulic potential and vapor pressure from the inferior of material through ambient in stage II drying

The total mass flux of water vapor due to evaporation (E) is calculated from the evaporation equation, i.e. a product of the water vapor concentration gradient near the evaporation surface defined as ($c_s - c_e$) as primary driving force and average mass-transfer coefficient ($\overline{h_m}$).

$$E = (c_s - c_e)\overline{h_m} \quad (1)$$

$$c_s = M.e_0/(RT) \text{ and } c_e = M.e_a/(RT) \quad (2)$$

where c_s is the water vapor concentration of the surface bleed water, or saturated water vapor concentration (kg/m^3) and c_e is the water vapor concentration in the air sufficiently far from the surface. M is the molar mass of the water (kg/mol), R is the universal gas constant (m^3.Pa/mol.K), and T is the absolute temperature (K). Parameters e_0 and e_a are the saturation water vapor pressure in the air immediately over the concrete surface, and water vapor pressure in the air surrounding the concrete (Pa), and analogous to the equation developed by Uno (Uno, 1998). The average mass-transfer coefficient ($\overline{h_m}$) is calculated from the diffusivity D (1/m^{2}s), and the characteristic length in the direction of the air flow, L (m) and represented as:

$$\overline{h_m} = \frac{\overline{Sh_L}\, D}{L} \quad (3)$$

$$\overline{Sh_L} = 0.6774\,\mathrm{Re}_L^{1/2}\, Sc^{1/3}\left[1+\left(\frac{0.0468}{Sc}\right)^{2/3}\right]^{-1/4} \qquad \mathrm{Re}_L < \mathrm{Re}_{crit} \quad (4)$$

$$\overline{Sh_L} = 0.6774\,\mathrm{Re}_{crit}^{1/2}\, Sc^{1/3}\left[1+\left(\frac{0.0468}{Sc}\right)^{2/3}\right]^{-1/4} + 0.037 Sc^{1/3}(\mathrm{Re}_L^{0.8} - \mathrm{Re}_{crit}^{0.8}) \qquad \mathrm{Re}_L < \mathrm{Re}_{crit} \quad (5)$$

The characteristic length (L) depends on the geometry. For example, for a flat plate, L is the distance from the leading edge or the length of slab in the direction of wind. Sherwood number ($\overline{Sh_L}$) as a function of Reynolds (R_L) and Schmidt (Sc) numbers, and represents combined effects of the wind velocity and temperature, or alternatively the ratio of the convective mass transfer to the rate of diffusive mass transport. Schmidt number (S_c) represents the ratio of momentum diffusivity (kinematic viscosity) and mass diffusivity, and is used to characterize fluid flows in which there are simultaneous momentum and mass diffusion convection processes. R_{crit} represents the critical Reynolds number for the flow over a flat water surface.

Average mass-transfer coefficient, $\overline{h_m}$, and temperature reflect the effect of characteristic length in the direction of the air flow. Diffusivity (D) is a function of temperature, and the water vapor concentration gradient near the evaporation surface ($c_s - c_e$) as shown in Fig. 6. Parametric studies shown in Fig. 7 reveal a concise effect of the temperature, RH and wind velocity on the evaporation rate. Additionally, effect of evaporation surface in the direction of wind flow on evaporation rates is studied and reduction of evaporation rate relates to increasing characteristic length. The parametric model was applied to the most recent experimental data by Slowik et al. (Slowik et al., 2008); Azenha et al. (Azenha et al., 2007a, 2007b); Lura et al. (Lura et al., 2007); and Hammer (Hammer, 2001).

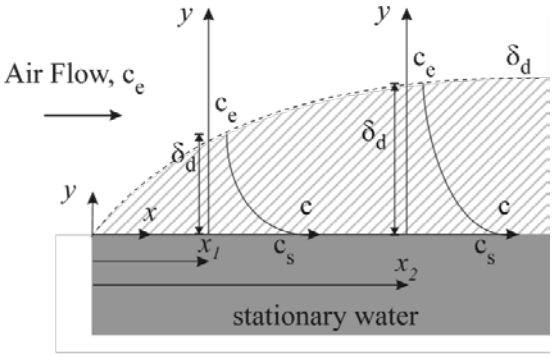

Fig. 6. Distribution of water vapor concentration and diffusion boundary layer thickness in laminar, and turbulent regions near concrete interface

4.0 MODELING OF THE SHRINKAGE RING SPECIMENS

Restrained shrinkage tests characterize the role of fibers in cracking potential using AASHTO PP34-99 test specimens ("AASHTO PP 34-99 Standard Practice for Estimating the Cracking Tendency of Concrete," 2005). While plastic shrinkage cracks are 2-D, a majority of modeling efforts address 1-D Mode I cracking by utilizing restraints (Lura *et al.*, 2007; Mora-Ruacho *et al.*, 2009).

Concrete with steel, AR glass, and PP fibers at V_f=0.1% were tested under restrained shrinkage cracking ASTM C 1579-13 (ASTM C1579-13, n.d.) by Rahmani *et al*. (Rahmani *et al.*, 2012). Maximum crack width and total crack area reduced by 30-50% and 40-60%, respectively, while first crack formation was delayed. Modeling was used to address observations (Soranakom *et al.*, 2008; Weiss *et al*., 2000). To simulate this response the components of a 1-D model are shown in Figs. 8 a, b and c. Fig. 8a shows the ring specimen; strain components (c) Concrete tensile stress strain and crack width model are shown in Figs. 8b and 8c respectively.

The shrinkage generates a compressive strain in the steel ring and tension in concrete and the friction between the concrete and steel due to clamping pressure. Cracking occurs when the tensile strain exceeds the allowable strain, and then opening of the crack relieves the stresses as shown in Figs. 9 (a-b). Creep of concrete in tension however allows for continuous load transfer. The input functions for modeling include free shrinkage at the outer surface, creep coefficients, concrete strength development and tensile stress strain relationship. The softening response of concrete continues to carry load in the post peak range as shown in Fig. 9a. Results indicate a significant reduction (up to 3 times less) in crack width using ARG-FRC and control specimens as shown in Fig. 9b. The strain response in the control sample after cracking indicates that concrete completely loses its ability to transfer the forces, while the ARG-FRC show strains in post-crack zone.

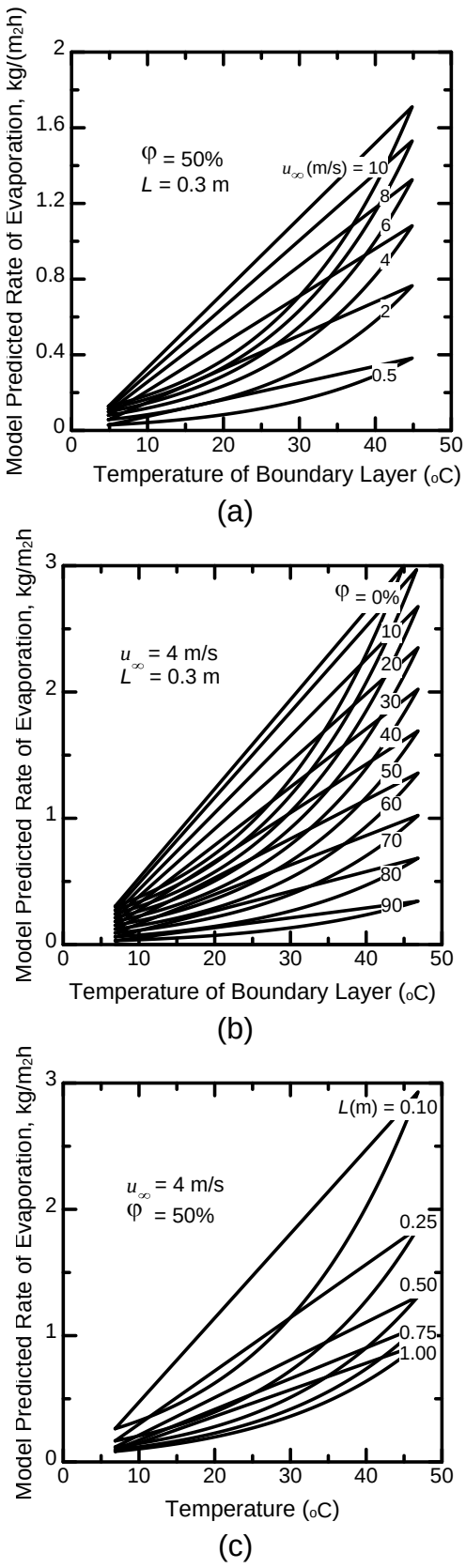

Fig. 7. Effect of boundary conditions (T, RH, wind, and characteristic length) on the rate of evaporation a) effect of wind velocity, b) effect of RH, c) effect of characteristic length (Slowik *et al.*, 2008)

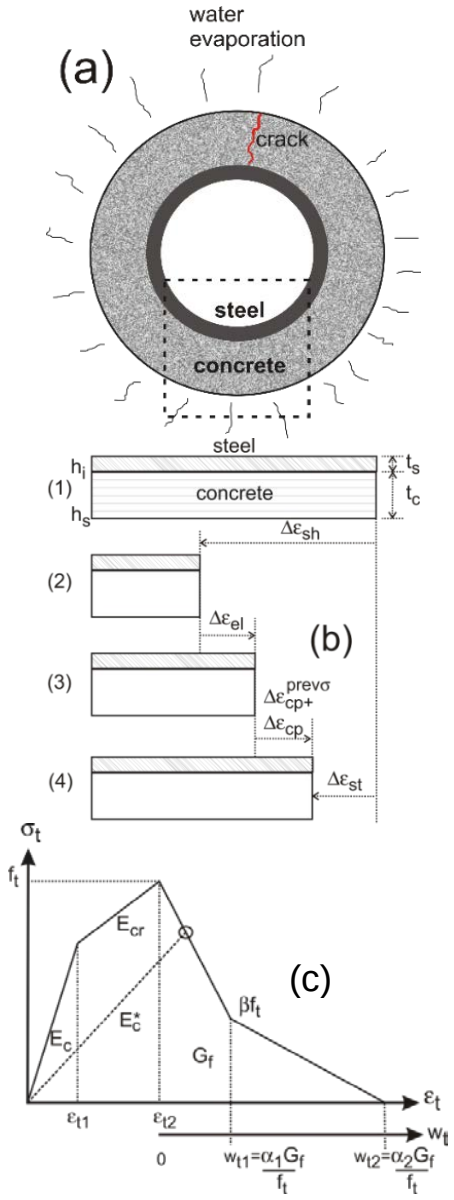

Fig. 8. Schematic drawing for drying shrinkage model; (a) ring specimen; (b) strain components (c) Concrete tensile stress strain and crack width model

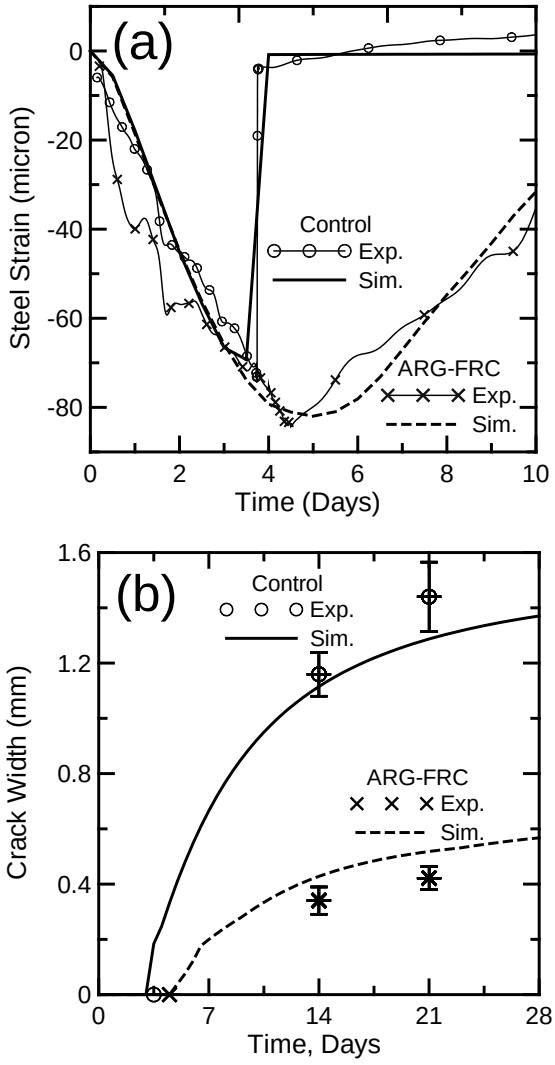

Fig. 9. Comparison between experimental result and model simulation; (a) strain history at steel ring; (b) crack width at outer concrete surface

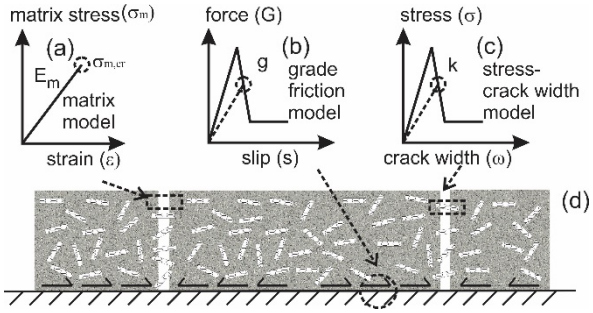

Fig. 10. Mechanical behavior of cracked FRC slab: **a)**matrix strength for cracking criterion, **b)**nonlinear spring model simulating the frictional force, **c** stress-crack width model, **d** cracked cement composite (Destrée *et al*., 2015).

5.0 OVERLAY SHRINKAGE CRACKING AND CURLING

This strain distribution in a slab is a combination of the shrinkage dominated mechanisms and the applied loads in the context of Euler-Bernoulli assumptions. From a structural point of view, one has to extend relevant microstructural parameters to the full slab that is bound by the joint and subbase restraint conditions as shown in Fig. 10. The strain distribution along the slab length and depth can be used to calculate slab cracking, joint opening, failure, and curling.

Numerical and empirical models addressing the drying shrinkage cracking behavior of joint-free steel-fiber-reinforced concrete (SFRC) slabs were studied by Destree *et al.* (Destrée *et al.*, 2015).

Using the schematic model shown in Figs. 11, a, b and c. A finite difference model to simulate the effect of shrinkage in consideration to the base support was developed and the numerical solution forms the basis and is extended to an empirical model for drying shrinkage cracking behavior of joint-free fiber-

reinforced concrete slabs. Fibers would allow for distribution of stresses and reduction of crack width such that the joint spacing can be increased significantly by as much as 100%.

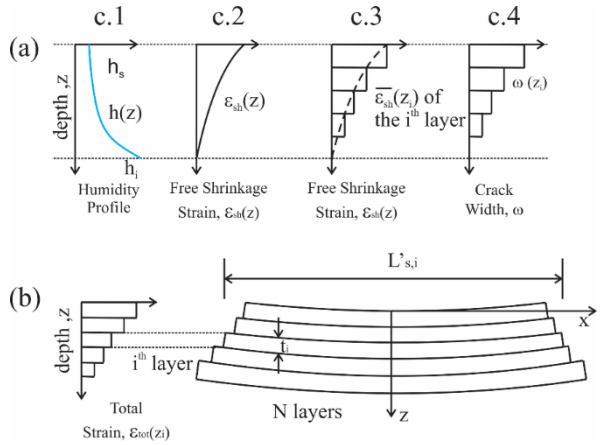

Fig. 11. Modelling procedure for curling of a slab. a) Slab strain distribution discretized into N layers and the impose strain gradient due to humidity profile. b) Distribution of total strain into the curvature and tip deflection (Destrée *et al*., 2015).

Using the finite-difference equilibrium solution of a one-dimensional (1D) slab on frictional ground, the formation of multiple cracks in the slab were calculated and compared with empirical crack opening models as shown in Fig. 12a Predicted crack opening as shown Fig. 12b reduces by increasing fiber volume, base friction, and interfacial bond strength. The model was extended to simulate the curling phenomenon in order to explain the corner slab lifting in service.

Effect of water-cement ratio, admixtures, free shrinkage, and mechanical restrictions including base friction were addressed. Fiber dosage, and interfacial bond properties restrain the growth of microcracks into main cracks and reduce crack opening. The modelling procedure to address the curling of a slab uses a discretized N layers through the thickness model and the stain gradient is imposed in each layer using the constant strain in each layer based on the distribution of total strain and curvature generated due to the differences in humidity as shown in Fig. 13. The tip deflection is obtained from the integration of curvature distribution. Tip deflection, or slab lift increases with smaller thickness and longer length of slab.

6.0 CONCLUSIONS

Various aspects of shrinkage cracking in cement-based materials are addressed. The drying rate of hydrating cement paste during hydration stages is studied using a method based on vacuum drying experiments and analytical procedures. Both micro and macro fibers affect the nature of restrained shrinkage cracking without altering the evaporation rate. Stages of microcrack coalescence due to plastic shrinkage cracking are analyzed using digital image correlation and a model for internal moisture transfer based on vapor diffusion is presented.

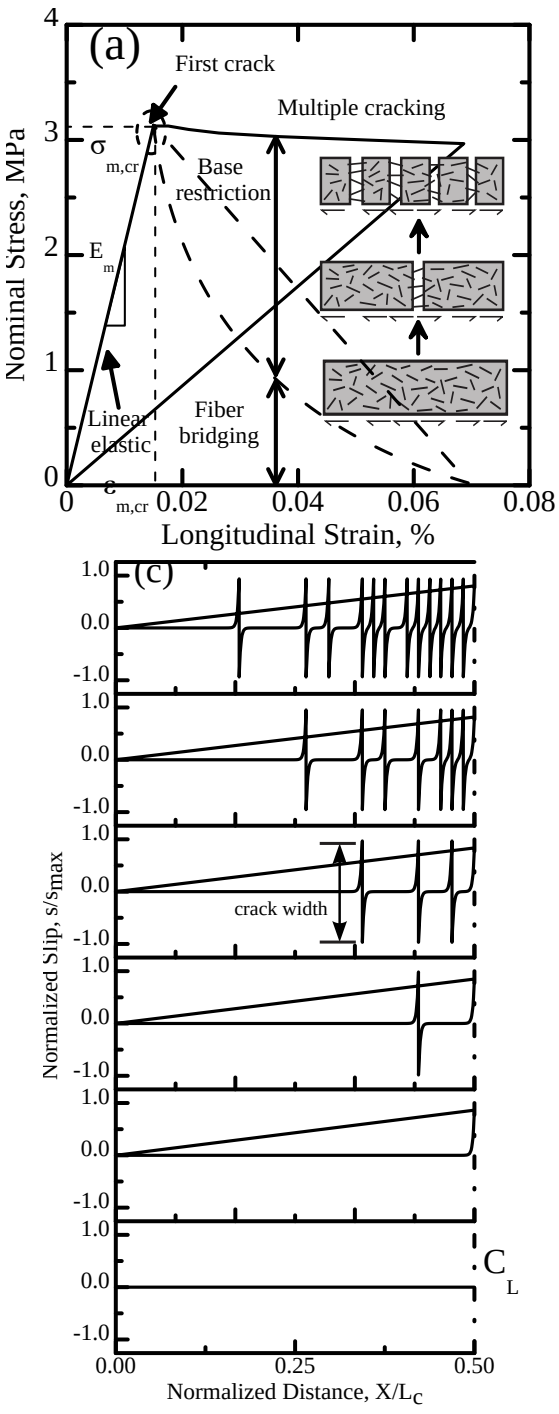

Fig. 12. (a) Stress-strain evaluation, and four normalized material responses of a numerical base model: (b) matrix stress distribution (Destrée *et al.*, 2015).

Effect of temperature, wind speed, and relative humidity are studied using fluid mechanics approach for water evaporation from the boundary-layer. Results are then integrated with an analytical approach for the restrained ring specimen as well as

a slab on ground in order to predict multiple transverse cracking as well as slab curling.

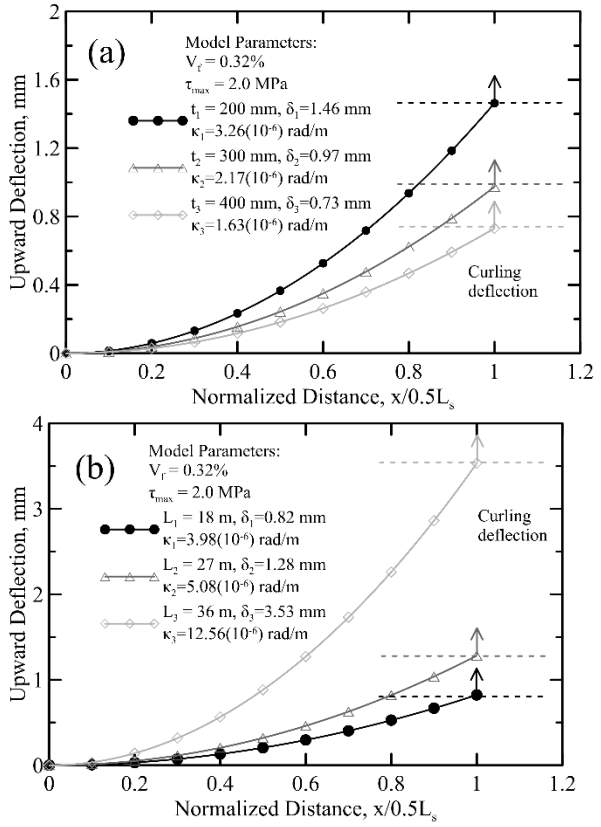

Fig. 13. Tip curling deflection increase at the cracked section with effect of slab thickness, and b) effect of slab length (Destrée *et al.*, 2015).

References

AASHTO PP 34-99 Standard Practice for Estimating the Cracking Tendency of Concrete, 2005.

ACI Committee 224, 2007. 224.1R-07 Causes, Evaluation, and Repair of Cracks in Concrete Structures.

ACI Committee 302, 2004. 302.1R-04: Guide for Concrete Floor and Slab Construction.

ACI Committee 544, 2010. 544.5R-10: Report on the Physical Properties and Durability of Fiber-Reinforced Concrete.

Arya, S.P., 2001. Introduction to Micrometeorology, International Geophysics. Academic Press, San Deigo, CA, United States.

ASTM C1579-13, n.d. Standard Test Method for Evaluating Plastic Shrinkage Cracking of Restrained Fiber Reinforced Concrete (Using a Steel Form Insert). ASTM International, West Conshohocken, PA.

Azenha, M., Maekawa, K., Ishida, T., Faria, R., 2007a. Drying induced moisture losses from mortar to the environment. Part I: experimental research. Mater Struct 40, 801–811. https://doi.org/10.1617/s11527-007-9244-y

Azenha, M., Maekawa, K., Ishida, T., Faria, R., 2007b. Drying induced moisture losses from mortar to the environment. Part II: numerical implementation. Mater Struct 40, 813–825. https://doi.org/10.1617/s11527-007-9243-z

Bakhshi M., Mobasher B., Zenouzi M., 2012. Model for Early-Age Rate of Evaporation of Cement-Based Materials. Journal of Engineering Mechanics 138, 1372–1380. https://doi.org/10.1061/(ASCE)EM.1943-7889.0000435

Banthia, N., Azzabi, M., Pigeon, M., 1993. Restrained shrinkage cracking in fibre-reinforced cementitious composites. Materials and Structures 26, 405–413. https://doi.org/10.1007/BF02472941

Banthia, N., Gupta, R., 2009. Plastic shrinkage cracking in cementitious repairs and overlays. Mater Struct 42, 567–579. https://doi.org/10.1617/s11527-008-9403-9

Banthia, N., Yan, C., 2000. Shrinkage Cracking in Polyolefin Fiber-Reinforced Concrete. MJ 97, 432–437. https://doi.org/10.14359/7406

Brighton, P.W.M., 1985. Evaporation from a plane liquid surface into a turbulent boundary layer. Journal of Fluid Mechanics 159, 323–345. https://doi.org/10.1017/S0022112085003238

Brutsaert, W., 1965. A model for evaporation as a molecular diffusion process into a turbulent atmosphere. Journal of Geophysical Research 70, 5017–5024. https://doi.org/10.1029/JZ070i020p05017

Carmeliet, J., Hens, H., Roels, S., Adan, O., Brocken, H., Cerny, R., Pavlik, Z., Hall, C., Kumaran, K., Pel, L., 2004. Determination of the Liquid Water Diffusivity from Transient Moisture Transfer Experiments. Journal of Thermal Envelope and Building Science 27, 277–305. https://doi.org/10.1177/1097196304042324

Cohen, M.D., Olek, J., Dolch, W.L., 1990. Mechanism of plastic shrinkage cracking in portland cement and portland cement-silica fume paste and mortar. Cement and Concrete Research 20, 103–119. https://doi.org/10.1016/0008-8846(90)90121-D

Destrée, X., Yao, Y., Mobasher, B., 2015. Sequential Cracking and Their Openings in Steel-Fiber-Reinforced Joint-Free Concrete Slabs. Journal of Materials in Civil Engineering 28. https://doi.org/10.1061/(ASCE)MT.1943-5533.0001377

Dey, V., Dakhane, A., Neithalath, N., Mobasher, B., 2015. Digital Image Correlation on a 2D Restrained Slab to Quantify the Early-Age Shrinkage Cracking Characteristics of Binder Systems. Presented at the ACI Fall Convention, Denver, CO, United States.

Dey V. Kachala R., Bonakdar A., Neithalath N. Mobasher B., 2016. Quantitative 2D Restrained Shrinkage Cracking of Cement Paste with Wollastonite Microfibers. Journal of Materials in Civil Engineering 28, 04016082. https://doi.org/10.1061/(ASCE)MT.1943-5533.0001592

Grzybowski, M., Shah, S.P., 1990. Shrinkage Cracking of Fiber Reinforced Concrete. MJ 87, 138–148. https://doi.org/10.14359/1951

Hammer, T.A., 2001. Effect of silica fume on the plastic shrinkage and pore water pressure of high-strength concretes. Mat. Struct. 34, 273–278. https://doi.org/10.1007/BF02482206

Huang, C.H., 1997. Pasquill's Influence: On the Evaporation from Various Liquids into the Atmosphere. J. Appl. Meteor. 36, 1021–1026. https://doi.org/10.1175/1520-0450(1997)0362.0.CO;2

Janz, M., 1997. Methods of measuring the moisture diffusivity at high moisture levels (Doctoral Thesis). University of Lund, Lund, Sweden.

Kim, J.-H.J., Park, C.-G., Lee, Si-Won, Lee, Sang-Woo, Won, J.-P., 2008. Effects of the geometry of recycled PET fiber reinforcement on shrinkage cracking of cement-based composites. Composites Part B: Engineering 39, 442–450. https://doi.org/10.1016/j.compositesb.2007.05.001

Kwon, S.J., Na, U.J., Park, S.S., Jung, S.H., 2009. Service life prediction of concrete wharves with early-aged crack: Probabilistic approach for chloride diffusion. Structural Safety 31, 75–83. https://doi.org/10.1016/j.strusafe.2008.03.004

Lura, P., Pease, B., Mazzotta, G.B., Rajabipour, F., Weiss, J., 2007. Influence of Shrinkage-Reducing Admixtures on Development of Plastic Shrinkage Cracks. MJ 104, 187–194. https://doi.org/10.14359/18582

Mora-Ruacho, J., Gettu, R., Aguado, A., 2009. Influence of shrinkage-reducing admixtures on the reduction of plastic shrinkage cracking in concrete. Cement and Concrete Research 39, 141–146. https://doi.org/10.1016/j.cemconres.2008.11.011

Mu, R., Forth, J. p., 2009. Modelling shrinkage of concrete from moisture lost using moisture diffusion theory. Magazine of Concrete Research 61, 491–497. https://doi.org/10.1680/macr.2008.00105

Prata, A.T., Sparrow, E.M., 1985. Diffusion-Driven Nonisothermal Evaporation. J. Heat Transfer 107, 239–242. https://doi.org/10.1115/1.3247384

Qi, C., Weiss, J., Olek, J., 2003. Characterization of plastic shrinkage cracking in fiber reinforced concrete using image analysis and a modified Weibull function. Mat. Struct. 36, 386–395. https://doi.org/10.1007/BF02481064

Rahmani, T., Kiani, B., Bakhshi, M., Shekarchizadeh, M., 2012. Application of Different Fibers to Reduce Plastic Shrinkage Cracking of Concrete, in: RILEM Bookseries. Presented at the 7th RILEM International Conference on Cracking in Pavements, Springer, Dordrecht, Netherland, pp. 635–642. https://doi.org/10.1007/978-94-007-4566-7_62

Slowik, V., Schmidt, M., Fritzsch, R., 2008. Capillary pressure in fresh cement-based materials and identification of the air entry value. Cement and Concrete Composites 30, 557–565. https://doi.org/10.1016/j.cemconcomp.2008.03.002

Soranakom, C., Bakhshi, M., Mobasher, B., 2008. Role of Alkali Resistant Glass Fibers in Suppression of Restrained Shrinkage Cracking of Concrete Materials. Presented at the 15th International Glass Fibre Reinforced Concrete Association Congress, GRC, Prague, Czech Republic.

Sultan, E., Boudaoud, A., Amar, M.B., 2005. Evaporation of a thin film: diffusion of the vapour and Marangoni instabilities. Journal of Fluid Mechanics 543, 183–202. https://doi.org/10.1017/S0022112005006348

Uno, P.J., 1998. Plastic Shrinkage Cracking and Evaporation Formulas. Aci Materials Journal 95, 365–375.

Weiss W. Jason, Yang Wei, Shah Surendra P., 2000. Influence of Specimen Size/Geometry on Shrinkage Cracking of Rings. Journal of Engineering Mechanics 126, 93–101. https://doi.org/10.1061/(ASCE)0733-9399(2000)126:1(93)

Yoon, I.S., Schlangen, E., de Rooij, M.R., van Breugel, K., 2007. The Effect of Cracks on Chloride Penetration into Concrete. Key Engineering Materials 348–349, 769–772.